



HAL
open science

Discontinuous enrichment in finite elements with a partition of unity method

John Dolbow, Nicolas Moës, Ted Belytschko

► **To cite this version:**

John Dolbow, Nicolas Moës, Ted Belytschko. Discontinuous enrichment in finite elements with a partition of unity method. *Finite Elements in Analysis and Design*, 2000, 36 (3-4), pp.235-260. 10.1016/S0168-874X(00)00035-4 . hal-01006752

HAL Id: hal-01006752

<https://hal.science/hal-01006752>

Submitted on 11 Jan 2023

HAL is a multi-disciplinary open access archive for the deposit and dissemination of scientific research documents, whether they are published or not. The documents may come from teaching and research institutions in France or abroad, or from public or private research centers.

L'archive ouverte pluridisciplinaire **HAL**, est destinée au dépôt et à la diffusion de documents scientifiques de niveau recherche, publiés ou non, émanant des établissements d'enseignement et de recherche français ou étrangers, des laboratoires publics ou privés.



Distributed under a Creative Commons Attribution - NonCommercial 4.0 International License

Discontinuous enrichment in finite elements with a partition of unity method

John Dolbow^{a,*}, Nicolas Moës^b, Ted Belytschko^b

^a*Department of Civil and Environmental Engineering, Duke University, Box 90287, Durham NC 27708-0287, USA*

^b*Mechanical Engineering, Northwestern University, USA*

A technique is presented to model arbitrary discontinuities in the finite element framework by locally enriching a displacement-based approximation through a partition of unity method. This technique allows discontinuities to be represented independently of element boundaries. The method is applied to fracture mechanics, in which crack discontinuities are represented using both a jump function and the asymptotic near-tip fields. As specific examples, we consider cracks and crack growth in two-dimensional elasticity and Mindlin–Reissner plates. A domain form of the J -integral is also derived to extract the moment intensity factors. The accuracy and utility of the method is also discussed.

Keywords: Discontinuous enrichment; Partition-of-unity; Fracture

1. Introduction

The modeling of evolving discontinuities with the finite element method is cumbersome due to the need to update the mesh topology to match the geometry of the discontinuity. In this paper, we present a technique to model discontinuities in the finite element framework in a general fashion. The essential feature is the incorporation of enrichment functions which contain a discontinuous field. In the application of the technique to fracture mechanics, functions spanning the appropriate near-tip crack field can also be included to improve accuracy. The enrichment of the finite element approximation in this manner provides for both the modeling of discontinuities and accurate moment intensity factors with minimal computational resources.

* Corresponding author. Fax: 1-919-660-5219.
E-mail address: jdolbow@duke.edu (J. Dolbow).

The concept of incorporating crack fields in a finite element context is not new, see for example [1]. In addition, there are several well-established techniques for modeling cracks and crack growth such as boundary element methods, finite elements with continuous remeshing [2], and meshless methods [3]. Recently, the trend has focused on the development of finite element methods which model discontinuities independently of element boundaries. These include the incorporation of a discontinuous mode in an assumed strain framework [4], and enrichment with near-tip fields for crack growth with minimal remeshing [5]. The latter method has recently been extended by enriching with a discontinuous function behind the crack tip [6,7], such that no remeshing is necessary.

In this paper, the method of discontinuous enrichment is cast in a general framework, and we illustrate how both two-dimensional and plate formulations can be enriched to model cracks and crack growth. The enrichment of the approximation with discontinuous near-tip fields requires a mapping technique, and so an alternative near-tip function is developed. The present method offers several advantages over competing techniques for modeling crack growth. In contrast to traditional finite element methods, this technique incorporates the discontinuity of the crack independently of the mesh, such that the crack can be arbitrarily located within an element. The present technique has a distinct advantage over boundary element methods as it is readily applicable to non-linear problems, anisotropic materials, and arbitrary geometries. The method does not require any remeshing for crack growth, and as it is an extension of the finite element method, it can exploit the large body of finite element technology and software. Specific examples of augmenting well established two-dimensional and plate elements with both discontinuous and asymptotic near-tip functions are presented.

The present technique exploits the partition of unity property of finite elements first cited by [8], which allows global enrichment functions to be locally incorporated into a finite element approximation. A standard approximation is ‘enriched’ in a region of interest by the global functions in conjunction with additional degrees of freedom and the local nodal shape functions. The application of this idea to capture a specific frequency band in dynamics can be found in [9]. The utility of the method has found application in solving the scalar Laplacian problem for domains with re-entrant corners [10]. In the context of fracture mechanics, the appropriate enrichment functions are the near-tip asymptotic fields and a discontinuous function to represent the jump in displacement across the crack line. In contrast to the work of [4], the enrichment is not through an assumed-strain method, so the displacement field is continuous along either side of the crack.

This paper is organized as follows. Following this introduction, we review the construction of an enriched approximation and we develop a discontinuous near-tip function which does not require a mapping. For specific applications we consider two-dimensional linear elastic fracture mechanics and the fracture of Mindlin–Reissner plates in Section 3. Numerical results to verify the accuracy of the formulation are given in Section 4, with a summary and some concluding remarks provided in the last section.

2. Construction of a finite element approximation with discontinuities

In this section, we present the construction of a finite element approximation with discontinuous enrichment. Emphasis is placed on modeling cracks, in which a standard approximation is

enriched with both the asymptotic near-tip functions and a discontinuous ‘jump’ function. The incorporation of discontinuous near-tip functions requires a mapping for kinked cracks, and so an alternative near-tip function is presented. The manner in which nodes are selected for enrichment and the modifications to the numerical integration of the weak form are also given.

2.1. General form

To introduce the concept of discontinuous enrichment, we begin by considering the domain Ω bounded by Γ with an internal boundary Γ_c as shown in Fig. 1a. We are interested in the construction of a finite element approximation to the field $\mathbf{u} \in \Omega$ which can be discontinuous along Γ_c .

Consider the uniform mesh of N nodes for the domain shown in Fig. 1b which does not model the discontinuity. The discrete approximation \mathbf{u}^h to the function \mathbf{u} takes the form

$$\mathbf{u}^h(\mathbf{x}) = \sum_I N_I(\xi(\mathbf{x}))\mathbf{u}_I, \quad (1)$$

where N_I is the shape function for node I in terms of the parent coordinates ($\xi(\mathbf{x})$), and \mathbf{u}_I is the vector of nodal degrees of freedom. The nodal shape function N_I is non-zero over the support of node I , defined to be union of the elements connected to the node.

We now pose the question of how to best incorporate the discontinuity in the field along Γ_c . The traditional approach is to change the mesh to conform to the line of discontinuity as shown in Fig. 1c, in which the element edges align with Γ_c . While this strategy certainly creates a discontinuity in the approximation, it is cumbersome if the line Γ_c evolves in time, or if several different configurations for Γ_c are to be considered.

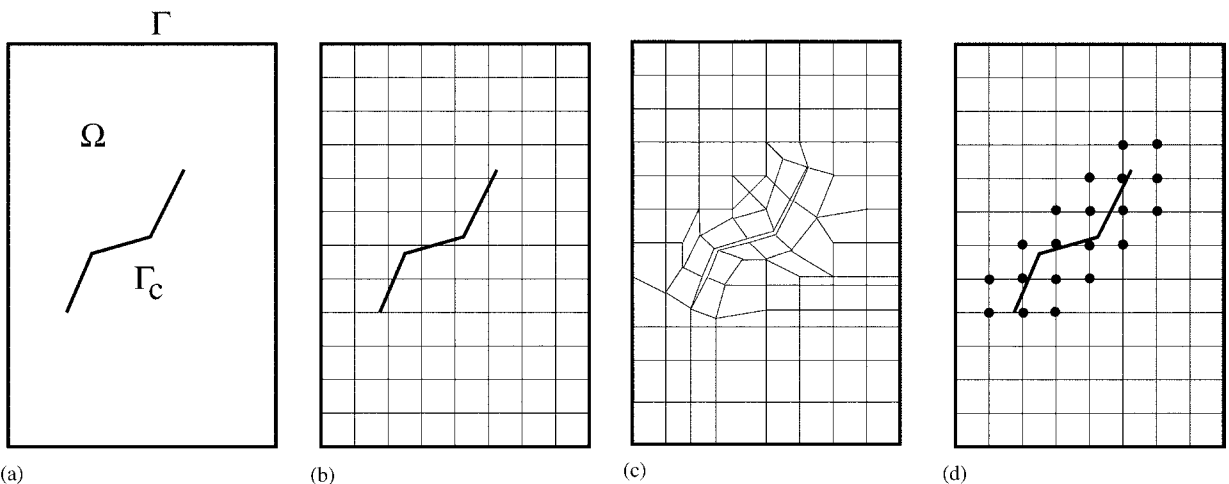


Fig. 1. Various discretizations for (a) a domain with an internal boundary Γ_c . (b) A mesh which does not model the internal boundary. (c) A mesh which conforms to the geometry of Γ_c . (d) A uniform mesh in which the circled nodes have additional degrees of freedom and enrichment functions.

In this paper we propose to model the discontinuity along Γ_c with *extrinsic enrichment* [11], in which the standard approximation (1) is modified as

$$\mathbf{u}^h(\mathbf{x}) = \sum_{I=1}^n N_I(\xi(\mathbf{x})) \left(\mathbf{u}_I + \sum_{l=1}^{n_E(I)} \mathbf{a}_{Il} G_l(\mathbf{x}) \right), \quad (2)$$

where $G_l(\mathbf{x})$ are enrichment functions, and \mathbf{a}_{Il} are additional nodal degrees of freedom for node I . In the above, the total number of enriched degrees of freedom for a node is denoted by $n_E(I)$. If the enrichment functions G_l are discontinuous along the boundary Γ_c , then the finite element mesh does not need to model the discontinuity. For example, the uniform mesh in Fig. 1d is capable of modeling a jump in \mathbf{u} when the circled nodes are enriched with functions which are discontinuous across Γ_c .

The above form of a finite element approximation merits some discussion. We note that the enrichment functions G_l are written in terms of the global coordinates \mathbf{x} , but that they are multiplied by the nodal shape functions N_I . In this fashion the additional enrichment takes on a local character. This concept of multiplying global functions by the finite element partition of unity was first suggested in [8]. The change in the form of the approximation from (1) to (2) is only made locally in the vicinity of a feature of interest, such as a discontinuity.

We now turn to the precise form of the enrichment functions used to model discontinuous fields, with the goal of modeling cracks and crack growth. Three distinct regions are identified for the crack geometry, namely the crack interior and the two near-tip regions as shown in Fig. 2. In the set I of all nodes in the mesh, we distinguish three different sets which correspond to each of these regions. The set J is taken to be the set of nodes enriched for the crack interior, and the sets K_1 and K_2 are those nodes enriched for the first and second crack tips, respectively. The precise manner in

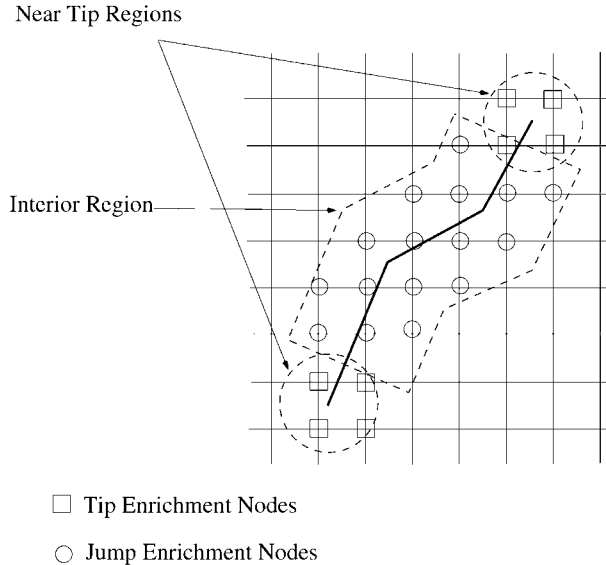


Fig. 2. Regions of a crack for enrichment. The circled nodes are enriched with a discontinuous function, while the squared nodes are enriched with near-tip functions.

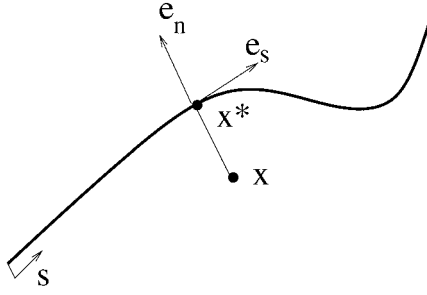


Fig. 3. Illustration of normal and tangential coordinates for a crack. \mathbf{x}^* is the closest point to \mathbf{x} on the crack. In the above case, the jump function $H(\mathbf{x}) = -1$.

which these sets are determined from the interaction of the crack and the mesh geometry is given in Section 2.3.

The enriched approximation takes the form

$$\mathbf{u}^h(\mathbf{x}) = \sum_I N_I \mathbf{u}_I + \sum_J N_J H(\mathbf{x}) \mathbf{b}_J + \sum_{K \in K_1} N_K \left(\sum_{l=1}^4 \mathbf{c}_{Kl}^1 F_l^1(\mathbf{x}) \right) + \sum_{K \in K_2} N_K \left(\sum_{l=1}^4 \mathbf{c}_{Kl}^2 F_l^2(\mathbf{x}) \right), \quad (3)$$

where \mathbf{b}_J and $\mathbf{c}_{Kl}^1, \mathbf{c}_{Kl}^2$ ($l = 1, \dots, 4$) are nodal degrees of freedom corresponding to the enrichment functions $H(\mathbf{x})$, $F_l^1(\mathbf{x})$ and $F_l^2(\mathbf{x})$, respectively. The function $H(\mathbf{x})$ is discontinuous across the crack line, and the sets $F_l^1(\mathbf{x})$ and $F_l^2(\mathbf{x})$ consist of those functions which span the near-tip asymptotic fields. For two-dimensional elasticity, these are given by

$$\{F_l(r, \theta)\}_{j=1}^4 \equiv \left\{ \sqrt{r} \sin\left(\frac{\theta}{2}\right), \sqrt{r} \cos\left(\frac{\theta}{2}\right), \sqrt{r} \sin\left(\frac{\theta}{2}\right) \sin(\theta), \sqrt{r} \cos\left(\frac{\theta}{2}\right) \sin(\theta) \right\}. \quad (4)$$

where (r, θ) are the local polar coordinates for the crack tip [12]. Note that the first function in (40), $\sqrt{r} \sin(\theta/2)$, is discontinuous across the crack faces whereas the last three functions are continuous. The form of the near-tip functions for plates is similar and is developed in Section 3.

The jump function $H(\mathbf{x})$ is defined as follows. The crack is considered to be a curve parametrized by the curvilinear coordinate s , as in Fig. 3. The origin of the curve is taken to coincide with one of the crack tips. Given a point \mathbf{x} in the domain, we denote by \mathbf{x}^* the closest point on the crack to \mathbf{x} . At \mathbf{x}^* , we construct the tangential and normal vector to the curve, \mathbf{e}_s and \mathbf{e}_n , with the orientation of \mathbf{e}_n taken such that $\mathbf{e}_s \wedge \mathbf{e}_n = \mathbf{e}_z$. The function $H(\mathbf{x})$ is then given by the sign of the scalar product $(\mathbf{x} - \mathbf{x}^*) \cdot \mathbf{e}_n$. In the case of a kinked crack, the cone of normals at \mathbf{x}^* needs to be considered (see [6]). Roughly speaking, the function $H(\mathbf{x})$ takes the value of 1 ‘above’ the crack, and -1 ‘below’ the crack.

2.2. An alternative near-tip function

The jump function $H(\mathbf{x})$ is in general not capable of representing the discontinuity in the displacement field along the entire crack geometry. For example, if the crack tip is not aligned with an element edge, then a near-tip function must also be used (see [6]). For cracks which are not straight, a mapping is required to align the near-tip discontinuities with the crack edges. Due to the

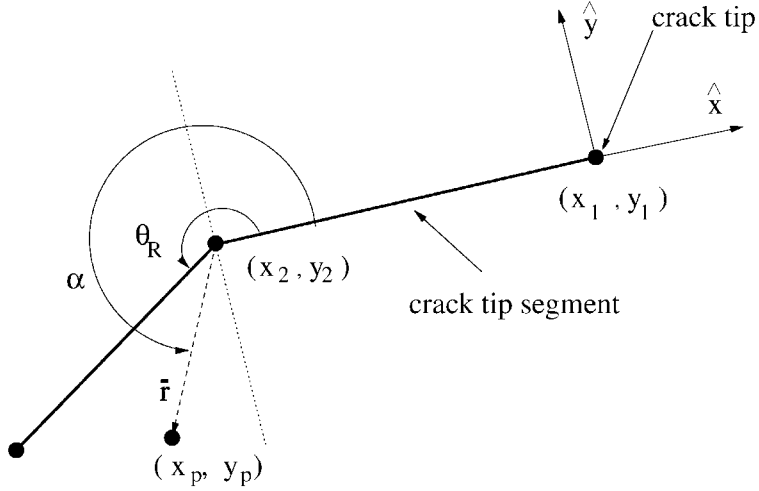


Fig. 4. Initial geometry for the mapping of the enrichment functions for the segment adjacent to the crack tip segment.

local form of the enrichment, the mapping procedure is only necessary in those elements with nodes enriched with the near-tip functions. In this section, we review the mapping procedure and present an alternative near-tip function.

The crack is modeled as a series of straight line segments connecting vertices, with new crack segments added as the crack grows. The discontinuities in the near-tip fields are aligned with each segment by using a procedure developed in [12,5]. In this procedure, the discontinuity in the near-tip functions are aligned with the crack by a mapping technique that rotates each section of the discontinuity onto the crack model.

A key step in technique is the modification of the angle θ in $F_I(r, \theta)$. Given a point (x_p, y_p) , we define an angle $\bar{\theta}(x_p, y_p)$ in terms of the angle of the segment θ_R (see Fig. 4) and the sampling point angle $\alpha(x_p, y_p)$ by

$$\bar{\theta} = \begin{cases} \left(\frac{\pi/2}{3\pi/2 - \theta_R} \right) (\alpha - \theta_R) & \text{for } \alpha > \theta_R, \\ \left(\frac{\pi/2}{\theta_R - \pi/2} \right) (\alpha - \theta_R) & \text{for } \alpha < \theta_R. \end{cases} \quad (5)$$

The coordinates of the sampling point (x_p, y_p) are mapped to coordinates in the crack tip frame (\hat{x}, \hat{y}) as shown in Fig. 5:

$$(\hat{x}_p, \hat{y}_p) = (-l - \bar{r} \cos(\bar{\theta}), -\bar{r} \sin(\bar{\theta})), \quad (6)$$

where l is the distance between (x_1, y_1) and (x_2, y_2) and \bar{r} is as shown in the figure. The variables r and θ in the enrichment functions are then computed in terms of the local (\hat{x}, \hat{y}) coordinates. This procedure is repeated similarly for each segment of the crack and the sequence of mappings leaves the length of the crack invariant.

In [5], the entire crack was modeled with the near-tip fields and the above mapping procedure. The use of the discontinuous function $H(\mathbf{x})$ eliminates the need for the mapping on the crack

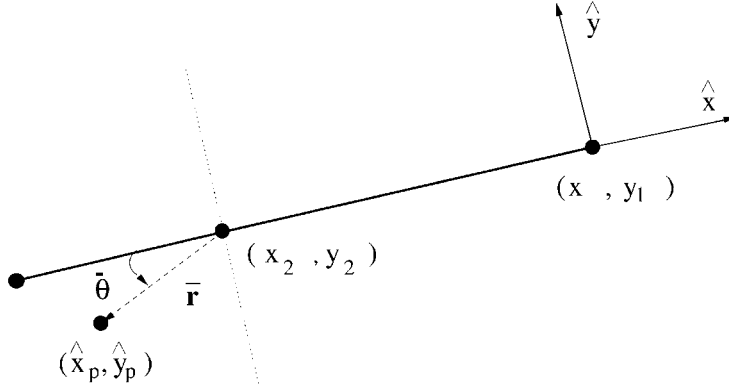


Fig. 5. The mapped point (x^*, y^*) used to determine r and θ in the near-tip functions $F_l(r, \theta)$.

interior, so that the above procedure is only necessary at each crack tip. In the following, we propose the use of a smooth ‘ramp’ function in conjunction with the function $H(\mathbf{x})$ to model the near-tip region.

Consider the following function defined in terms of the crack tip coordinates (\hat{x}, \hat{y}) :

$$R(\hat{x}, \hat{y}) = \begin{cases} 3\left(\frac{\hat{x}}{l_c}\right)^2 + 2\left(\frac{\hat{x}}{l_c}\right)^3 & \text{for } \hat{x} \leq 0, \\ 0 & \text{for } \hat{x} > 0, \end{cases} \quad (7)$$

where the length l_c is taken to be the characteristic length of the element containing the crack tip. The above function and its derivative vanishes at the crack tip.

When this smooth ramp function is multiplied by the function $H(\mathbf{x})$, i.e.,

$$\tilde{R}(\mathbf{x}) = R(\hat{x}, \hat{y}) \cdot H(\mathbf{x}) \quad (8)$$

a near-tip function which is discontinuous across the crack edges and vanishes in front of the crack tip results. This function in turn does not require any mapping to align the discontinuity with the crack edges. The function \tilde{R} is shown in Fig. 6 in the vicinity of a crack tip and two consecutive segments. It is clear from the figure that the resulting near-tip function is continuous in the domain Ω and discontinuous across the crack line.

The above near-tip function is useful on several levels. In the first instance, in conjunction with the function $H(\mathbf{x})$ for the crack interior it is perhaps the simplest means to model the entire crack discontinuity. In addition, for non-linear problems the exact near-tip functions may not be known. The concept of multiplying a smooth function which vanishes at the crack tip by the jump function $H(\mathbf{x})$ can also be extended to three-dimensional problems. In linear elastic fracture mechanics, however, the incorporation of the asymptotic near-tip fields is still useful to obtain greater accuracy at the crack tip. To some extent, this advantage can be maintained by simply replacing the first function in (4) with the function \tilde{R} :

$$\{F_l(r, \theta)\}_{j=1}^4 \equiv \left\{ R(\hat{x}, \hat{y})H(\mathbf{x}), \sqrt{r} \cos\left(\frac{\theta}{2}\right), \sqrt{r} \sin\left(\frac{\theta}{2}\right) \sin(\theta), \sqrt{r} \cos\left(\frac{\theta}{2}\right) \sin(\theta) \right\}. \quad (9)$$

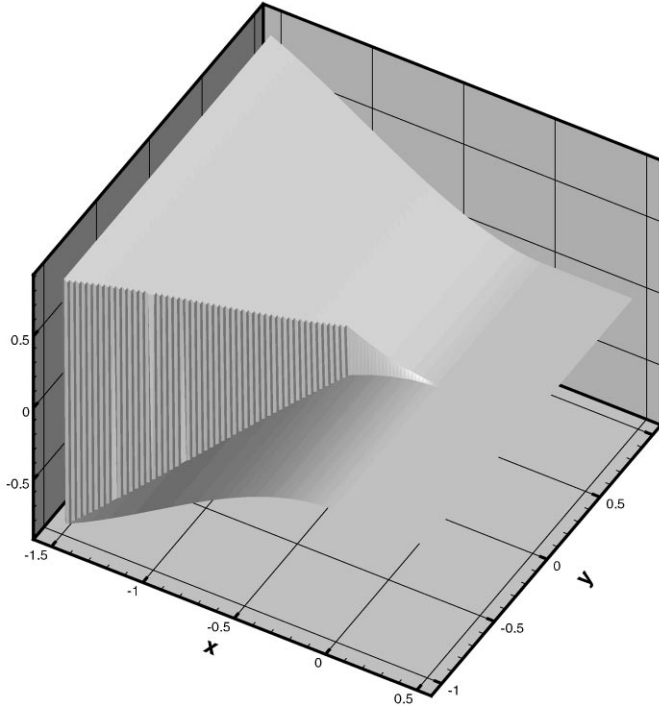


Fig. 6. Surface plot of near-tip function $\tilde{R}(x)$ in an element. The crack tip is located at $(x, y) = (0.0, 0.0)$ with a crack vertex at $(-0.5, 0.0)$.

The last three functions need not be mapped into the crack faces, as they are all continuous in the domain Ω .

2.3. Node selection for enrichment

In the preceding development, three distinct regions were identified for enrichment, corresponding to the nodal sets J , K_1 and K_2 . In this section we define these sets precisely, and present the methodology by which nodes are identified for inclusion in each set.

We begin with some preliminary notations. The support of node I is denoted by ω_I , with closure $\bar{\omega}_I$. Essentially, a node's support is the open set of element domains connected to the node, and the closure is the closed set which includes the outer boundary. The distinction as it applies to nodal selection will be discussed shortly. We also denote the location of crack tips 1 and 2 by \mathbf{x}_1 and \mathbf{x}_2 respectively, and by C the geometry of the crack.

With these definitions, the sets J , K_1 and K_2 are defined as follows. The sets K_1 and K_2 consist of those nodes whose support closure contains crack tip 1 or 2, respectively. The set J is the set of nodes whose support is intersected by the crack and do not belong to K_1 or K_2 :

$$K_1 = \{k \in I: \mathbf{x}_1 \in \bar{\omega}_k\}, \quad (10)$$

$$K_2 = \{k \in I: \mathbf{x}_2 \in \bar{\omega}_k\}, \quad (11)$$

$$J = \{j \in I: \omega_j \cap C \neq \emptyset, j \notin K_1, j \notin K_2\}. \quad (12)$$

Note that the set J consists of nodes whose support, as opposed to support closure, is intersected by the crack. This distinction implies that if the crack only intersects the boundary of a node's support, the node will not be enriched with the function $H(\mathbf{x})$. This prevents any nodes from being enriched with a constant function (either -1 or $+1$) over their entire support, which is important in order to avoid creating a linear dependency in the approximation. We note that for the alternative near-tip function proposed in the previous section, the support closure must be changed to the open set for similar reasons.

In practice the above sets are determined as follows. All elements intersected by the crack are first determined. From this set of elements, we distinguish three disjoint sets of 'tip elements' (for either tip 1 or 2) and 'interior elements'. The set of tip elements are given by those which contain either crack tip. The nodes of the 'tip elements' correspond to either set K_1 or K_2 . The nodes of the 'interior elements' in turn correspond to the set J . Fig. 7 illustrates the nodes that are selected as tip nodes and interior nodes for the cases of a uniform mesh and an unstructured mesh.

An additional step is taken to remove those nodes from the set J whose support closure, but not support, is intersected by the crack. For this purpose, subpolygons which align with both the crack and element boundaries are generated as shown in Fig. 8b. These subpolygons are generated easily enough by triangulating the polygons formed from the intersection of the crack and element boundaries.

The generation of the subtriangles allows the computation of the amount of a node's support 'above' and 'below' the crack, which can then be compared against a tolerance. In two-dimensional analysis, we denote the area of a nodal support by A_ω , which is calculated from the sum of the areas of each element connected to the node. With the aid of the subtriangles, we also calculate the nodal support area above A_ω^{ab} and below A_ω^{be} the crack. We then calculate the ratios

$$r_{\text{above}} = \frac{A_\omega^{\text{ab}}}{A_\omega}, \quad (13a)$$

$$r_{\text{below}} = \frac{A_\omega^{\text{be}}}{A_\omega}. \quad (13b)$$

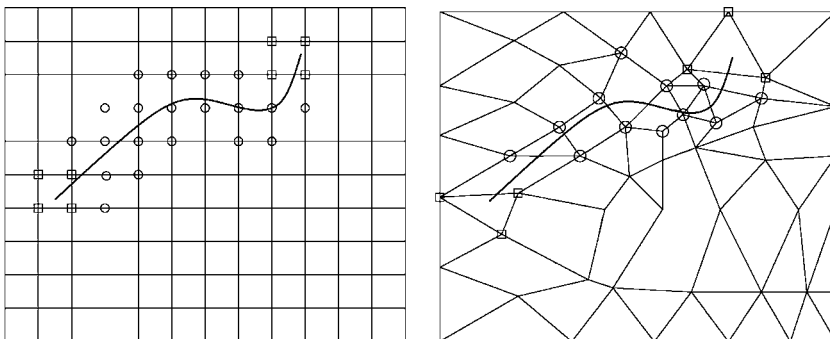


Fig. 7. Crack on a uniform mesh (left) and on a non-uniform mesh (right). The circled nodes are enriched by the jump function whereas the squared nodes are enriched by the crack tip functions.

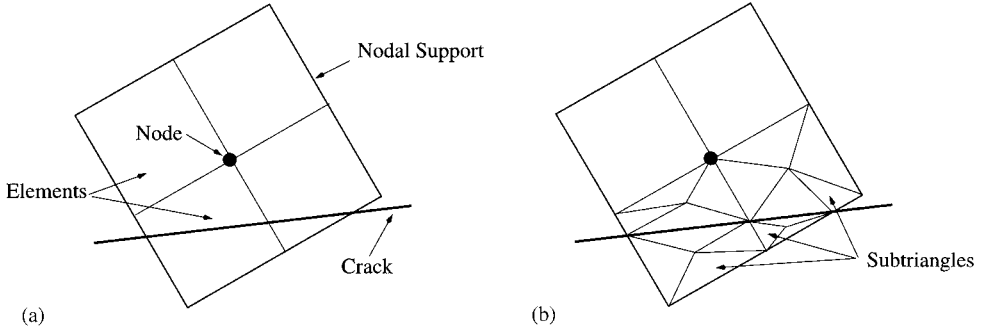


Fig. 8. (a) Nodal support cut by a crack. (b) The subtriangles associated with elements cut by the crack for node selection and the numerical integration of the weak form.

If either of these ratios are below a tolerance (we have used 0.01, or 1%), the nodes are removed from the set J .

2.4. Numerical integration of the weak form

For elements cut by the crack and enriched with the jump function $H(\mathbf{x})$, we make a modification to the element quadrature routines for the assembly of the weak form. As the crack is allowed to be arbitrarily oriented in an element, standard Gauss quadrature may not adequately integrate the discontinuous field. For those nodes in the set J , it is important that the quadrature scheme accurately integrate the contributions to the weak form on both sides of the discontinuity. If the integration of the discontinuous enrichment is indistinguishable from that of a constant function, spurious singular modes can appear in the system of equations. In this section, we present the modifications made to the numerical integration scheme for elements cut by a crack.

The discrete weak form is normally constructed with a loop over all elements, as the domain is approximated by

$$\bar{\Omega} = \bigcup_{e=1}^m \bar{\Omega}_e, \quad (14)$$

where m is the number of elements, and $\bar{\Omega}_e$ is the element subdomain. For elements cut by a crack, we define the element subdomain to be a union of a set of subpolygons whose boundaries align with the crack geometry

$$\bar{\Omega}_e = \bigcup_{s=1}^{m_s^e} \bar{\Omega}_s \quad (15)$$

where m_s^e denotes the number of subpolygons for the element. The subtriangles shown in Fig. 8 already generated for the selection of the interior nodes also work well for integration. It is emphasized that the subpolygons are only necessary for integration purposes; no additional degrees of freedom are associated with their construction. In the integration of the weak form, the element loop is replaced by a loop over the subpolygons for those elements cut by the crack.

3. Application to fracture mechanics

In this section, we review the pertinent equations for linear elastic fracture mechanics. In this paper, emphasis is placed on plate fracture, although some two-dimensional plane-strain studies are discussed. A key difference in the plate formulation is the enrichment of the displacement components with different sets of near-tip functions. After reviewing the governing equations for Mindlin–Reissner plates, we examine the form of the asymptotic crack tip fields. A domain form of the J -integral for plates is derived for the calculation of the energy release rate and the moment intensity factors. Finally, the enriched finite element approximation is presented.

3.1. Mindlin–Reissner plate formulation

Two main formulations exist to model a plate: the classical theory or Kirchhoff plate theory and the Mindlin–Reissner plate theory. Allowing three boundary conditions instead of two for the Kirchhoff theory, the Mindlin theory gives a more realistic shear and moment distribution around a crack tip (see [13,14]). A summary of the Mindlin theory follows.

3.1.1. Governing equations

There are several different ways to introduce the Mindlin theory. As we are also interested in examining problems in two-dimensional elasticity, the theory is presented here as a degeneration of the three-dimensional elasticity problem using the principle of virtual work with the appropriate kinematic assumptions.

Consider a plate of thickness t whose mid-plane lies in the x_1 – x_2 Cartesian plane. The conventions used throughout this paper are shown in Fig. 9. The main assumptions of the Mindlin theory state that the in-plane displacements, u_1 and u_2 vary linearly through the thickness with the section rotations ψ_1 and ψ_2 . In addition, the normal stress σ_{33} is assumed to vanish in the domain. For the sake of simplicity, we make the additional assumptions that the surface of the plate and any crack faces are traction free.

In the $(\mathbf{e}_1, \mathbf{e}_2, \mathbf{e}_3)$ basis, where \mathbf{e}_3 is the unit normal vector to the plate, the deformation components at a point (x_1, x_2, x_3) are given by

$$\mathbf{u}(\mathbf{x}) = \begin{cases} u_1 = x_3 \psi_1(x_1, x_2), \\ u_2 = x_3 \psi_2(x_1, x_2), \\ u_3 = w(x_1, x_2), \end{cases} \quad (16)$$

where w is the transverse displacement and ψ_1 and ψ_2 are the rotations about the x_2 and x_1 axes, respectively. The above can be expressed in a more compact form as

$$\mathbf{u}(\mathbf{x}) = w \mathbf{e}_3 + x_3 \boldsymbol{\psi}, \quad (17)$$

where $\boldsymbol{\psi} = \psi_1 \mathbf{e}_1 + \psi_2 \mathbf{e}_2$.

The strain is given by

$$\frac{1}{2}(\nabla \mathbf{u} + (\nabla \mathbf{u})^t) = x_3 \boldsymbol{\varepsilon}_b(\boldsymbol{\psi}) + \frac{1}{2}(\boldsymbol{\varepsilon}_s(w, \boldsymbol{\psi}) \otimes \mathbf{e}_3 + \mathbf{e}_3 \otimes \boldsymbol{\varepsilon}_s(w, \boldsymbol{\psi})) \quad (18)$$

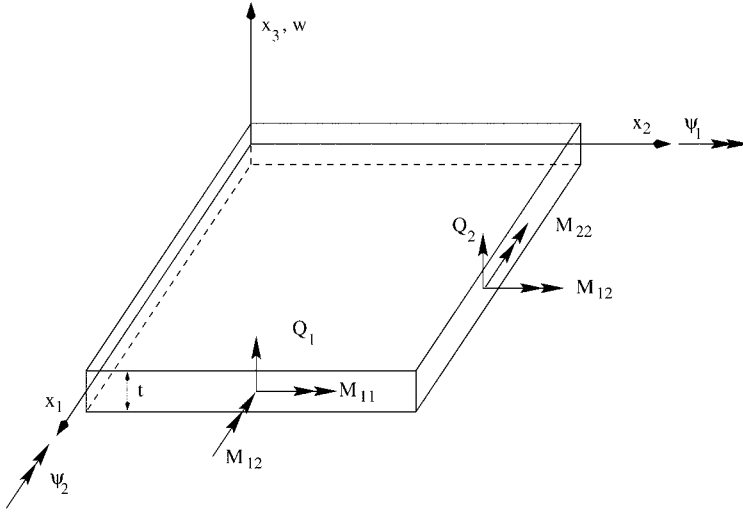


Fig. 9. Notations and sign conventions for a plate.

with the bending contribution

$$\boldsymbol{\varepsilon}_b(\boldsymbol{\psi}) = \frac{1}{2}(\nabla\boldsymbol{\psi} + (\nabla\boldsymbol{\psi})^t) \quad (19)$$

and a shear contribution

$$\boldsymbol{\varepsilon}_s(w, \boldsymbol{\psi}) = \nabla w + \boldsymbol{\psi}. \quad (20)$$

We note that the x_3 related components are zero for both $\boldsymbol{\varepsilon}_b$ and $\boldsymbol{\varepsilon}_s$.

The virtual internal work is defined by

$$\delta W^{\text{int}} = \int_{\Omega} \boldsymbol{\sigma} : \nabla(\delta \boldsymbol{u}) \, d\Omega \quad (21)$$

where $\boldsymbol{\sigma}$ is the symmetric stress tensor, and $\delta \boldsymbol{u}$ is an arbitrary virtual displacement from the current position. After a few manipulations, we obtain the relation

$$\boldsymbol{\sigma} : \nabla(\delta \boldsymbol{u}) = x_3 \boldsymbol{\sigma}^\pi : \boldsymbol{\varepsilon}_b(\delta \boldsymbol{\psi}) + \boldsymbol{\sigma}^s \cdot \boldsymbol{\varepsilon}_s(\delta w, \delta \boldsymbol{\psi}) \quad (22)$$

where the π superscript indicates a reduction of the operator to the in plane (x_1, x_2) component and $\boldsymbol{\sigma}^s$ is the shear stress vector $\boldsymbol{\sigma}^s = \boldsymbol{\sigma} \cdot \boldsymbol{e}_3$.

Making substitution (22) into (21) and integrating through the thickness gives the work expression

$$\delta W^{\text{int}} = \int_A (\boldsymbol{M} : \boldsymbol{\varepsilon}_b(\boldsymbol{\psi}) + \boldsymbol{Q} \cdot \boldsymbol{\varepsilon}_s(w, \boldsymbol{\psi})) \, dA, \quad (23)$$

where the moment \mathbf{M} and shear \mathbf{Q} are defined by

$$\mathbf{M} = \int_{-t/2}^{t/2} x_3 \boldsymbol{\sigma}^\pi dx_3 \quad \mathbf{Q} = \int_{-t/2}^{t/2} \boldsymbol{\sigma}^s dx_3. \quad (24)$$

The virtual external work is composed of the action of the bending and twisting moments gathered in a couple vector \mathbf{C} , and of the shear traction \mathbf{T} . We assume there is no external pressure acting on the plate. The virtual external work is then given by

$$\delta W^{\text{ext}} = \int_{\Gamma} \mathbf{C} \cdot \delta \boldsymbol{\psi} d\Gamma + \int_{\Gamma} \mathbf{T} \delta w d\Gamma. \quad (25)$$

Equating the internal and external virtual work, and applying the divergence theorem yields the equilibrium equations in Ω

$$\nabla \cdot \mathbf{M} - \mathbf{Q} = 0, \quad (26a)$$

$$\nabla \cdot \mathbf{Q} = 0 \quad (26b)$$

and the traction boundary conditions on Γ

$$\mathbf{C} = \mathbf{M} \cdot \mathbf{n}, \quad (27a)$$

$$\mathbf{T} = \mathbf{Q} \cdot \mathbf{n}, \quad (27b)$$

where \mathbf{n} is the unit outward normal to the boundary.

The constitutive relationships are obtained by energetic equivalence between the plate and the three-dimensional model. Assuming the plate is made of an isotropic homogeneous elastic material of Young's modulus E and of Poisson's ratio ν , the constitutive relations are given by

$$\begin{bmatrix} M_{11} \\ M_{22} \\ M_{12} \end{bmatrix} = \frac{Et^3}{12(1-\nu^2)} \begin{bmatrix} 1 & \nu & 0 \\ \nu & 1 & 0 \\ 0 & 0 & 1-\nu \end{bmatrix} \begin{bmatrix} \varepsilon_{b11} \\ \varepsilon_{b22} \\ \varepsilon_{b12} \end{bmatrix} \quad (28)$$

and

$$\begin{bmatrix} Q_1 \\ Q_2 \end{bmatrix} = \frac{Ekt}{2(1+\nu)} \begin{bmatrix} \varepsilon_{s1} \\ \varepsilon_{s2} \end{bmatrix}, \quad (29)$$

where $k = \frac{5}{6}$ is a correction factor which accounts for the parabolic variation of the shear stresses through the plate thickness.

These are rewritten in a more compact form using the fourth-order bending stiffness tensor \mathbf{D}_b and the second-order shear stiffness tensor \mathbf{D}_s :

$$\mathbf{M} = \mathbf{D}_b \boldsymbol{\varepsilon}_b \quad \mathbf{Q} = \mathbf{D}_s \boldsymbol{\varepsilon}_s. \quad (30)$$

3.1.2. Weak form

Let the boundary Γ be divided into a part Γ_u on which displacement boundary conditions are imposed and a part Γ_t on which loads are applied with the restrictions

$$\Gamma = \Gamma_u \cup \Gamma_t, \quad \Gamma_u \cap \Gamma_t = \emptyset. \quad (31)$$

The kinematics constraints are given by a prescribed transverse displacement w and prescribed rotations $\boldsymbol{\psi}$ while the loads come from the prescribed couples \mathbf{C} and prescribed shear tractions \mathbf{T} . As in Section 2, we also designate Γ_c as an internal boundary across which the displacement field is allowed to be discontinuous.

Let \mathcal{V}_g be the space of kinematically admissible transverse displacements and rotations

$$\mathcal{V}_g = \{(w, \boldsymbol{\psi}) \in \mathcal{V} : w = w_g, \boldsymbol{\psi} = \boldsymbol{\psi}_g \text{ on } \Gamma_u\}, \quad (32)$$

where \mathcal{V} is a space of sufficiently smooth functions on Ω . The details on this matter when the domain contains an internal boundary or re-entrant corner may be found in [15,16]. We note that the space \mathcal{V} allows for discontinuous functions across the crack line.

The space of test functions is defined similarly as

$$\mathcal{V}_0 = \{(w, \boldsymbol{\psi}) \in \mathcal{V} : w = 0, \boldsymbol{\psi} = 0 \text{ on } \Gamma_u\}. \quad (33)$$

The weak form is to find $(w, \boldsymbol{\psi}) \in \mathcal{V}_g$ such that

$$\begin{aligned} & \int_{\Omega} (\mathbf{D}_b \boldsymbol{\varepsilon}(\boldsymbol{\psi})) : \boldsymbol{\varepsilon}(\delta\boldsymbol{\psi}) \, d\Omega + \int_{\Omega} (\mathbf{D}_s \mathbf{s}(w, \boldsymbol{\psi})) \cdot \mathbf{s}(\delta w, \delta\boldsymbol{\psi}) \, d\Omega \\ & = \int_{\Gamma} \mathbf{C} \cdot \delta\boldsymbol{\psi} \, d\Gamma + \int_{\Gamma} \mathbf{T} \delta w \, d\Gamma \quad \forall (\delta w, \delta\boldsymbol{\psi}) \in \mathcal{V}_0. \end{aligned} \quad (34)$$

It can be shown that the above is equivalent to the equilibrium equations (26) and traction boundary conditions (27). When the space \mathcal{V} is discontinuous along Γ_c , the traction-free conditions on the crack faces are also satisfied. In contrast to boundary element techniques, this enables the method to be easily extended to non-linear problems.

In the finite element method, the space \mathcal{V} is approximated with a finite-dimensional space $\mathcal{V}^h \subset \mathcal{V}$. The space \mathcal{V}^h is typically made discontinuous across Γ_c by explicitly meshing the surface, as in Fig. 1c. In the present method, the approximating space is constructed with discontinuous enrichment.

3.2. Plate fracture mechanics

Consider the problem of a through crack in a plate as shown in Fig. 10, where for convenience we adopt a local polar coordinate system centered at the crack tip. In contrast to the stress intensity factors obtained in classical linear elasticity, in plate theory the quantities of interest are moment and shear force intensity factors. The moment intensity factors are denoted by K_{I} and K_{II} , while the shear force intensity factor is denoted by K_{III} . These are defined as

$$K_{\text{I}} = \lim_{r \rightarrow 0} \sqrt{2r} M_{22}(r, 0), \quad K_{\text{II}} = \lim_{r \rightarrow 0} \sqrt{2r} M_{12}(r, 0), \quad (35)$$

$$K_{\text{III}} = \lim_{r \rightarrow 0} \sqrt{2r} Q_2(r, 0). \quad (36)$$

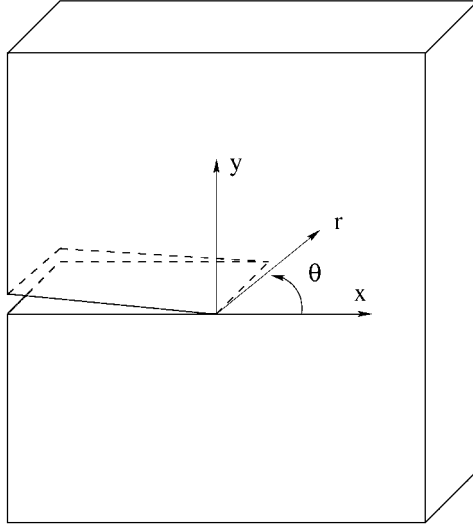


Fig. 10. Local polar coordinate system for a through crack in a plate.

The relationship between these factors and the energy release rate G is similar to the three-dimensional theory

$$G = \frac{12\pi}{Et^3}[K_I^2 + K_{II}^2] + \frac{6\pi}{5Et}K_{III}^2. \quad (37)$$

The form of the asymptotic near-tip displacement fields differs significantly from the three-dimensional theory. In particular, the transverse displacement w is only singular when a K_{III} mode is present. The asymptotic displacement fields in Mindlin–Reissner plate theory are given in [17], and they are provided here for the sake of completeness.

$$\begin{aligned} w = & \frac{6\sqrt{2r}}{5h\mu} K_3 \sin\left(\frac{\theta}{2}\right) \\ & + \frac{6\sqrt{2r^{3/2}}K_1}{Eh^3} \left[\frac{1}{3} (7 + \nu)\cos\left(\frac{3\theta}{2}\right) - (1 - \nu)\cos\left(\frac{\theta}{2}\right) \right] \\ & + \frac{6\sqrt{2r^{3/2}}K_2}{Eh^3} \left[-\frac{1}{3} (5 + 3\nu)\sin\left(\frac{3\theta}{2}\right) + (1 - \nu)\sin\left(\frac{\theta}{2}\right) \right], \end{aligned} \quad (38a)$$

$$\begin{aligned} \psi_1 = & \frac{6\sqrt{2r}K_1}{Eh^3} \cos\left(\frac{\theta}{2}\right) [4 - (1 + \nu)(1 + \cos(\theta))] \\ & + \frac{6\sqrt{2r}K_2}{Eh^3} \sin\left(\frac{\theta}{2}\right) [4 + (1 + \nu)(1 + \cos(\theta))] \\ & + \frac{6\sqrt{2r^{3/2}}K_3}{Eh^3} \frac{8}{15} \left[-\sin\left(\frac{\theta}{2}\right) - (1 + 3\nu)\cos\left(\frac{\theta}{2}\right)\sin(\theta) \right], \end{aligned} \quad (38b)$$

$$\begin{aligned}
\psi_2 = & \frac{6\sqrt{2r}K_1}{Eh^3} \left[4 \sin\left(\frac{\theta}{2}\right) - (1 + \nu) \left(\cos\left(\frac{\theta}{2}\right) \sin(\theta) \right) \right] \\
& + \frac{6\sqrt{2r}K_2}{Eh^3} \left[-2 \cos\left(\frac{\theta}{2}\right) (1 - \nu) + (1 + \nu) \sin\left(\frac{\theta}{2}\right) \sin(\theta) \right] \\
& + \frac{6\sqrt{2r^{3/2}}K_3}{Eh^3} \frac{8}{15} \cos\left(\frac{\theta}{2}\right) [1 + (1 + 3\nu)\cos(\theta)].
\end{aligned} \tag{38c}$$

For the purposes of defining the near-tip enrichment functions in the plate theory, we consider only the terms proportional to \sqrt{r} for the rotations ψ_1 and ψ_2 . For the transverse displacement, we consider terms proportional to both \sqrt{r} and $r^{3/2}$. With these restrictions, the near-tip fields are contained in the span of the sets

$$w \in \{g_i(r, \theta)\}_{i=1}^5, \tag{39a}$$

$$\{\psi_1, \psi_2\} \in \{f_i(r, \theta)\}_{i=1}^4, \tag{39b}$$

where

$$\{g_I(r, \theta)\} \equiv \left\{ \sqrt{r} \sin\left(\frac{\theta}{2}\right), r^{3/2} \sin\left(\frac{\theta}{2}\right), r^{3/2} \cos\left(\frac{\theta}{2}\right), r^{3/2} \sin\left(\frac{3\theta}{2}\right), r^{3/2} \cos\left(\frac{3\theta}{2}\right) \right\}, \tag{40a}$$

$$\{f_I(r, \theta)\} \equiv \left\{ \sqrt{r} \sin\left(\frac{\theta}{2}\right), \sqrt{r} \cos\left(\frac{\theta}{2}\right), \sqrt{r} \sin\left(\frac{\theta}{2}\right) \sin(\theta), \sqrt{r} \cos\left(\frac{\theta}{2}\right) \sin(\theta) \right\}. \tag{40b}$$

The discrete approximation for the plate which incorporates the above near-tip functions is presented in Section 3.4.

3.3. Domain form of the J -integral

Several different domain and path-independent integrals have been developed for the extraction of mixed mode moment and shear force intensity factors in plates [17]. These integrals typically consist of a contour integral enclosing the crack-tip singularity. With finite elements, the numerical evaluation of these integrals usually involves some kind of smoothing technique, as the required field quantities are discontinuous at element interfaces.

In this section, we illustrate the use of a weighting function q to recast these line integrals into their equivalent domain form. The development presented here closely follows that given for two-dimensional elasticity in [18]. The domain forms of crack contour integrals are particularly well suited for use with finite elements, as the same quadrature points used for the integration of the weak form can be used to calculate the domain integral. The construction of additional quadrature points or the use of a smoothing procedure is not required.

Consider the open contour Γ surrounding a through crack as shown in Fig. 11. In the following, we use indicial notation where the Greek indices (α, β) range over the values 1, ..., 2, and a comma denotes a derivative with respect to the following argument. The contour integral proposed by [17]

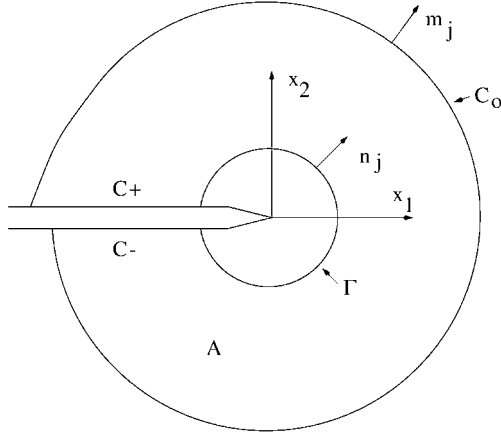


Fig. 11. Conventions at the crack tip for the domain form of the J -integral.

in the absence of an externally applied pressure is given by

$$J_1 = \oint_{\Gamma} \{W\delta_{1\beta} - [M_{\alpha\beta}\psi_{\alpha,1} + Q_{\beta}w_{,1}]\}n_{\beta} d\Gamma, \quad (41)$$

where W is the strain energy density of the plate. This is defined as

$$W = \frac{1}{2}[M_{\alpha\beta}\psi_{\alpha,\beta} + Q_{\beta}(\psi_{\beta} + w_{,\beta})]. \quad (42)$$

We now introduce a weight function q_1 which is defined over the domain of interest. Consider the simply connected curve $C = C_0 + C_+ + C_- + \Gamma$ as shown in Fig. 11. The function q_1 is defined to be sufficiently smooth in the area A enclosed by C , and is given on the surfaces by

$$q_1 = \begin{cases} 1 & \text{on } \Gamma, \\ 0 & \text{on } C_0. \end{cases} \quad (43)$$

We then use this function to rewrite (41) as

$$J_1 = \oint_C \{ -W\delta_{1\beta} + [M_{\alpha\beta}\psi_{\alpha,1} + Q_{\beta}w_{,1}] \} m_{\beta} q_1 dC \\ - \int_{C_+ + C_-} [M_{\alpha 2}\psi_{\alpha,1} + Q_2 w_{,1}] m_2 q_1 dC, \quad (44)$$

where we have used $m_i = n_i$ on C_0 , $m_i = -n_i$ on Γ , and $m_1 = 0$, $m_2 = + - 1$ on the crack faces. The last integral above vanishes for traction-free crack faces. Applying the divergence theorem to the closed integral, we then obtain

$$J_1 = \int_A \{ [M_{\alpha\beta}\psi_{\alpha,1} + Q_{\beta}w_{,1}] - W\delta_{1\beta} \} q_{1,\beta} dA - \int_{C_+ + C_-} [M_{\alpha 2}\psi_{\alpha,1} + Q_2 w_{,1}] m_2 q_1 dC, \quad (45)$$

which is the equivalent domain form of the J_1 integral proposed by [17].

The measure number J_I is domain independent and its magnitude is equivalent to the energy release rate (37). Therefore, under pure mode I loading, the moment intensity factor K_I is given by

$$K_I = \sqrt{\frac{Et^3}{12\pi}} G \quad (46)$$

In more general mixed-mode conditions, the values K_I , K_{II} and K_{III} cannot be separated so easily. While the comparison of J_I to analytical values is adequate to assess the effectiveness and qualities of the enrichment strategy, crack growth laws are typically expressed in terms of the mixed-mode intensity factors. In classical linear elasticity, the interaction integral approach [19] has proven effective to extract mixed-mode stress intensity factors. The application of this method to plate fracture is currently under development [20].

3.4. Enrichment of the MITC4 plate element

When discretizing the plate equations (26), some care must be taken to avoid shear locking. As the plate becomes very thin (i.e. $t \rightarrow 0$), the following relationship must be satisfied to keep the strain energy in the plate bounded:

$$\nabla w + \psi = 0. \quad (47)$$

In other words, the shear strain ϵ_s must vanish as $t \rightarrow 0$. Standard displacement-based elements, such as the four-node isoparametric element, have difficulty satisfying this constraint. The consequence is a structure which exhibits an overly stiff response, often referred to as shear locking.

To discretize the plate displacements (16), we begin with the MITC4 element. To avoid shear locking, the MITC formulation modifies the approximation for the section rotations ψ in the expression for the shear stiffness (see [21]). In the following, we express this modification using the notation \tilde{N}_I , where it is understood that only those expressions relating to the shear components are modified.

The enriched discretization takes the form

$$w^h(\mathbf{x}) = \sum_{I=1}^4 N_I w_I + \sum_J N_J H(\mathbf{x}) b_J^w + \sum_K N_K \left(\sum_{l=1}^4 c_{KI}^w G_l(r, \theta) \right), \quad (48a)$$

$$\psi^h(\mathbf{x}) = \sum_{I=1}^4 \tilde{N}_I \psi_I + \sum_J \tilde{N}_J H(\mathbf{x}) b_J^\psi + \sum_K N_K \left(\sum_{l=1}^4 c_{KI}^\psi F_l(r, \theta) \right), \quad (48b)$$

where N_I are the standard bilinear shape functions. In the above, we have collapsed the sums over each crack tip into one for compactness.

The sets of near-tip functions G_l and F_l are derived from (40) in the following fashion. We take G_l to be only those functions in g_l which are proportional to $r^{3/2}$. The set F_l is taken to be equivalent to f_l . In addition to having four additional degrees of freedom for each displacement component, this choice for G_l and F_l satisfies the following relation:

$$\nabla G_l(r, \theta) \in \text{span } F_l(r, \theta), \quad (49)$$

such that a linear combination of the near-tip enrichment functions can satisfy (47). We note that this relationship does not ensure that the enriched formulation will be completely free of shear locking. However, the numerical examples presented in the next section indicate that the above formulation performs well for a wide range of plate thicknesses.

4. Numerical examples

In this section we present several different numerical calculations. We first examine some problems in two-dimensional elasticity, including a robustness test and the simulation of crack growth. Then a benchmark and an additional study are presented for Mindlin–Reissner plates.

4.1. Two-dimensional problems

We begin with a simple example of an edge crack to demonstrate the robustness of the discretization scheme, and then present results for more complicated geometries. In all of the following examples, the material is taken to be isotropic with Young’s modulus $E = 200$ GPa, and Poisson’s ratio $\nu = 0.3$, and plane strain conditions are assumed. The calculation of the stress intensity factors is performed with the domain form of the interaction integral, and the maximum hoop stress law is used to govern crack growth (see [19,5]).

4.1.1. Robustness tests

Consider the geometry shown in Fig. 12: a plate of width w and height L with an edge crack of length a , subjected to a far-field stress σ^0 . We analyze the influence of the location of the crack with respect to the mesh on the K_I stress intensity factor when the position of the crack is perturbed by δx in the X direction and δy in the Y direction. The geometry is discretized with a uniform mesh of 24×48 4-noded quadrilateral elements.

In this study, several different discretizations are obtained depending on the position of the crack with respect to the mesh. Two cases are shown in Fig. 13. In this investigation, we wish to examine the performance of the modified tip function $\tilde{R}(\mathbf{x})$, and the accuracy of the formulation when it is used in conjunction with the other near-tip functions as in (9).

The exact solution for this problem is given by [22]

$$K_I = C\sigma\sqrt{a\pi} \quad (50)$$

where C is a finite-geometry correction factor

$$C = 1.12 - 0.231\left(\frac{a}{W}\right) + 10.55\left(\frac{a}{W}\right)^2 - 21.72\left(\frac{a}{W}\right)^3 + 30.39\left(\frac{a}{W}\right)^4. \quad (51)$$

The numerical results normalized by the exact solution when only the function $\tilde{R}(\mathbf{x})$ is used to model the near-tip region are given in Table 1. Depending on the location of the crack tip, the total number of degrees of freedom varies from 2483 to 2503. The results vary by approximately 4% over all crack tip locations tested. When the near-tip functions are added, the accuracy improves as

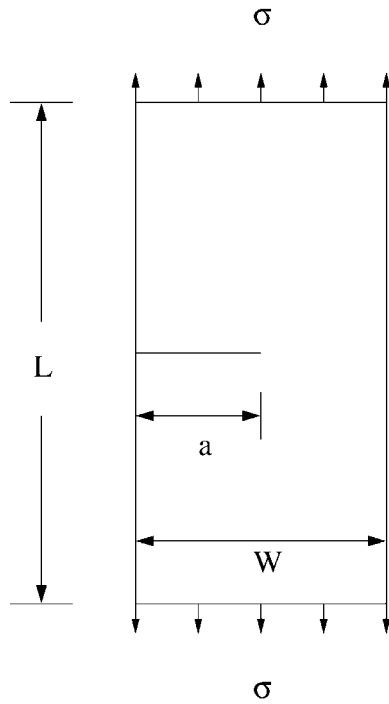


Fig. 12. The geometry of the edge crack problem for the robustness and shear studies. The parameters are $a/W = \frac{1}{2}$, $L/W = 16/7$, $W = 7$.

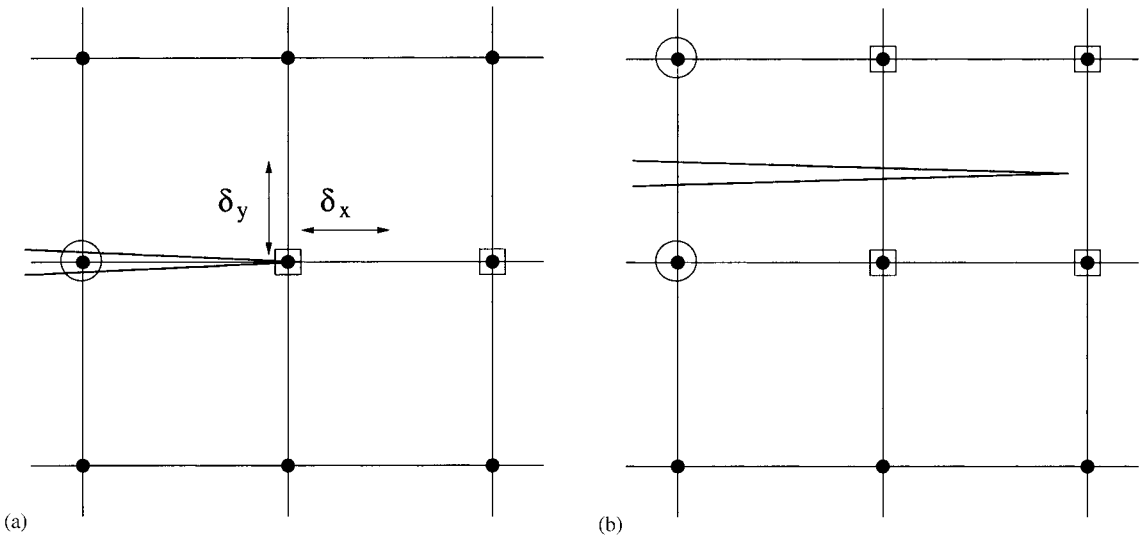


Fig. 13. Zoom of the mesh in the vicinity of the crack tip, with (a) the initial configuration and δ_x , δ_y shown. The enrichment is also shown for (b) the final configuration. The circled nodes are enriched with the jump function and the squared nodes with the near-tip functions.

Table 1

Normalized K_I values for various crack tip positions using near-tip function $\tilde{R}(x)$

δ_y/h_y	δ_x/h_x				
	0.171	0.343	0.514	0.686	0.857
-0.60	0.924	0.910	0.914	0.909	0.918
-0.30	0.925	0.912	0.914	0.911	0.919
0.0	0.942	0.939	0.948	0.952	0.949
0.30	0.925	0.913	0.915	0.911	0.919
0.60	0.923	0.909	0.914	0.909	0.918

Table 2

Normalized K_I values for various crack tip positions using near-tip functions $\tilde{R}(x)$ and $f(r, \theta)$

δ_y/h_y	δ_x/h_x				
	0.171	0.343	0.514	0.686	0.857
-0.60	0.945	0.939	0.954	0.936	0.941
-0.30	0.945	0.937	0.948	0.937	0.941
0.0	0.955	0.950	0.961	0.970	0.960
0.30	0.945	0.939	0.949	0.937	0.941
0.60	0.944	0.937	0.954	0.936	0.942

shown in Table 2. These results are consistent with those reported in [6] in that the best results are obtained when the crack is aligned with mesh boundaries. We note that the results are not as accurate as when the exact asymptotic function $\sqrt{r} \sin(\theta)$ is used, in which case the error is less than 2% (see [6]).

4.1.2. Crack growth from a fillet

This example shows the growth of a crack from a fillet in a structural member, and serves to illustrate how the present method can be used as an aid to design against failure. The configuration to be studied is shown in Fig. 14, with the actual domain modeled as indicated. The setup is taken from experimental work found in [23]. In this example, we investigate the effect of the thickness of the lower I-beam on crack growth. Only the limiting cases for the bottom I-beam of a rigid constraint (very thick beam) and flexible constraint (very thin beam) are considered. In addition, the welding residual stresses between the member and the I-beam are neglected.

The structure is loaded with a traction of $P = 20.0$ kN, and the initial crack length is taken to be $a_0 = 5$ mm. The geometry is discretized with 8243 three-node triangular elements. To model a rigid constraint, the displacement in the vertical direction is fixed along the entire bottom of the domain. A flexible constraint is idealized by fixing the vertical displacement at both ends of the bottom of

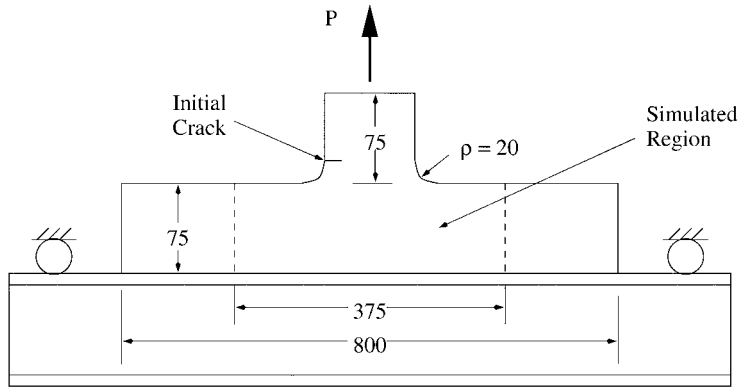


Fig. 14. Experimental configuration for crack growth problem.

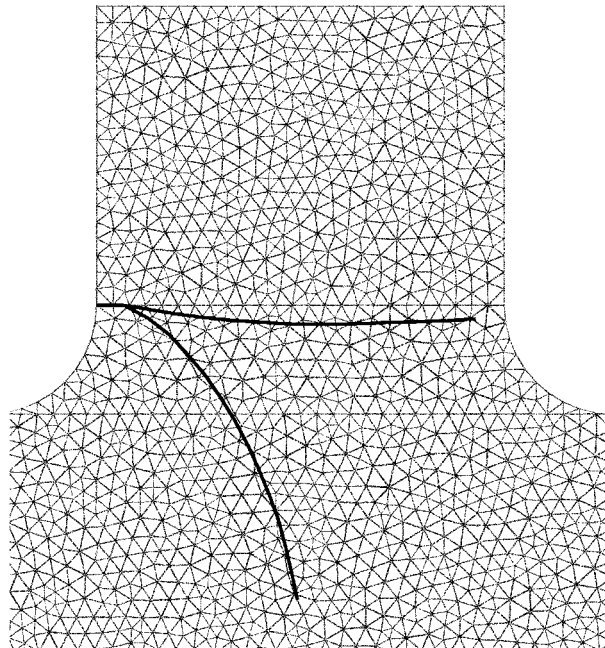


Fig. 15. Zoom of the crack paths (thick lines) for the cases of a rigid (top crack) and flexible (bottom crack) I-beam.

the domain. For both sets of boundary conditions, an additional degree of freedom is fixed to prevent a rigid-body rotation.

For each load case, we simulate crack growth with a step size of $\Delta a = 5$ mm for a total of 14 steps. Fig. 15 shows the mesh in the vicinity of the fillet and compares the crack paths for the cases of a thick I-beam (upper crack) and a thin I-beam (lower crack). It is emphasized that the same mesh is used throughout the simulation, and that no remeshing is required. As new crack segments are added, additional enriched degrees of freedom are generated for each new segment. The results shown are consistent with both the experimental [23] and previous numerical results [24].

4.2. Plate examples

In this section, we present some examples using the enriched MITC4 plate formulation developed in Section 3.4). We first examine the accuracy of the method as a function of plate thicknesses for a benchmark problem, and then present a more general example. Throughout this section, the material properties are assumed to be isotropic with Young's modulus of $E = 200$ GPa, and Poisson's ratio $\nu = 0.3$.

As a benchmark problem we consider a through crack in an infinite plate subjected to a far-field moment M_0 . The crack is oriented at an angle β with respect to the x_1 axis as shown in Fig. 16. Recently, very accurate calculations were carried out by [25] for various plate thicknesses for the case when $\beta = 0^\circ$. In this case, the loading is purely mode I, and the domain form of the J -integral for plates (45) is used in conjunction with (46) to determine the moment intensity factor K_I . In the finite element model, only one-half of a square plate is modeled, with symmetry conditions along the x_2 axis. To approximate the infinite plate, the plate width w is taken to be 10 times the half crack length a . The crack length for all of the results presented in this section is taken to be $2a = 1.0$.

Fig. 17 shows the normalized K_I for four discretizations, two standard and two enriched. The lower curve corresponds to a non-enriched formulation, and the values for K_I are within 5% of the exact for the entire range of plate thicknesses t . These values are improved when the mesh is refined for a total of 2463 degrees of freedom as shown. We observe that the enriched solution with only 755 degrees of freedom is as accurate as the solution with 2463 degrees of freedom without enrichment. The last curve for the enriched case with 3087 degrees of freedom exhibits less than 1% error. The enriched solutions show good correlation with the analytical solution for the full range of plate thicknesses tested.

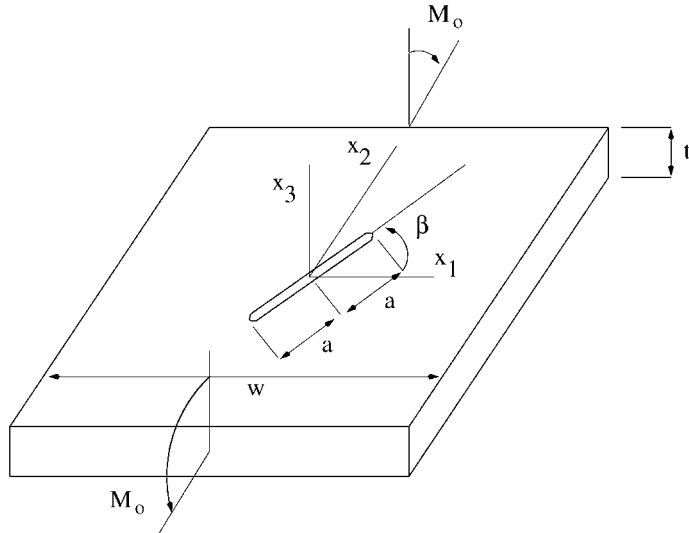


Fig. 16. Loading configuration for bending of cracked plate.

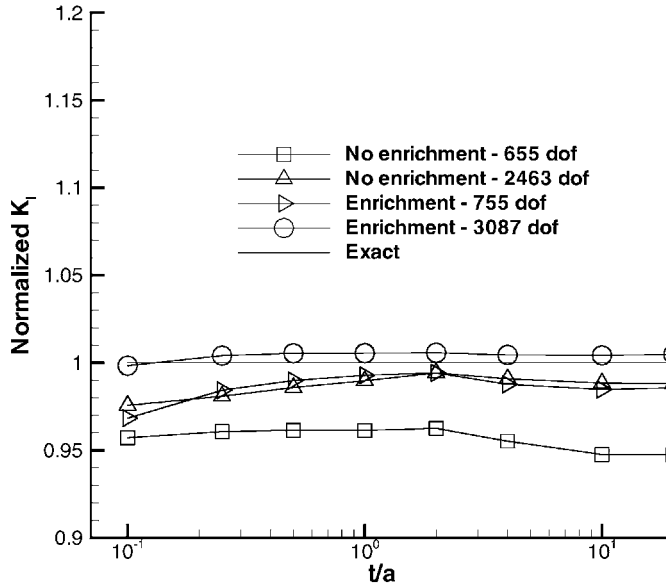


Fig. 17. Normalized moment intensity factors for varying plate thickness.

Table 3

Normalized K_I values for finite plate

$t = w/4$		$t = w/8$		$t = w/12$		$t = w/16$	
$\frac{a}{w}$	$\frac{K_I}{K_I^{\text{exact}}}$	$\frac{a}{w}$	$\frac{K_I}{K_I^{\text{exact}}}$	$\frac{a}{w}$	$\frac{K_I}{K_I^{\text{exact}}}$	$\frac{a}{w}$	$\frac{K_I}{K_I^{\text{exact}}}$
0.025	0.988	0.025	0.989	0.0333	1.067	0.0250	1.077
0.05	0.992	0.050	0.993	0.0500	1.052	0.0375	1.090
0.10	0.997	0.075	0.995	0.0667	1.069	0.0500	1.094
0.20	1.000	0.100	0.996	0.0833	1.070	0.0625	1.092
0.25	0.999	0.125	0.997	0.1667	1.054	0.1250	1.072
0.333	1.013	0.250	0.998	0.3333	1.057	0.2500	1.062

As a last example, moment intensity factors are calculated for a finite plate as a function of crack length for various plate thicknesses. The geometry of the plate is taken to be the same as the previous example, and the results are compared to those given in [26]. In this study, the mesh does not model the crack discontinuity; the jump in the rotations and transverse displacement is created entirely with enrichment. Table 3 gives the results for four different plate width-to-thickness ratios for the case when the plate is modeled with 1424 MITC4 elements. These results show excellent correlation for the cases when $t = w/4$ and $w/8$, in which the maximum error is 1.2%. For the remaining cases the maximum difference between the numerical solutions and those given in [26] is

9.4%. We note, however, that Ref. [26] is not as current as [25]. In the latter, the moment intensity factors are shown to be significantly greater than the classical results as the thickness $t \rightarrow 0$. The results shown in Table 3 are consistent with these findings.

5. Summary

A method of constructing finite element approximations with enrichment functions was presented which allows for the simulation of evolving discontinuities in a straightforward fashion. The specific examples of cracks and crack growth in two-dimensional elasticity and Mindlin–Reissner plate theory were examined. By incorporating the appropriate asymptotic near-tip fields, accurate moment and stress intensity factors were obtained for coarse meshes. A new near-tip function was also developed to remove the need for a mapping in the case of kinked cracks. The methodology for the construction of the discrete approximation from the interaction of the crack geometry and the mesh was provided, and numerical tests served to illustrate the algorithm’s robustness. Additional numerical studies for Mindlin–Reissner plates demonstrated the extent to which stress intensity factors can be calculated accurately for a wide range of plate thicknesses.

The present method has a lot of potential to extend the finite element method for the modeling of evolving interfaces and free surfaces. A key feature of the enrichment in conjunction with numerical integration is the capability of modeling geometrical features which are independent of the mesh topology. As was shown in this paper, several different crack configurations can be considered for a single mesh of a component, simply by changing the enrichment scheme according to the crack geometry. Future work will focus on the application of the method to three-dimensional and dynamic fracture, as well as other areas of mechanics in which moving interfaces are of importance.

Acknowledgements

The support of the Office of Naval Research and Army Research Office, to Northwestern University, is gratefully acknowledged. The authors are grateful for the support provided by the DOE Computational Science Graduate Fellowship program, to John Dolbow.

References

- [1] P. Tong, T. Pian, S. Lasry, A hybrid-element approach to crack problems in plane elasticity, *Int. J. Numer. Methods Eng.* 7 (1973) 297–308.
- [2] D. Swenson, A. Ingrassia, Modeling mixed-mode dynamic crack propagation using finite elements: theory and applications, *Comput. Mech.* 3 (1988) 381–397.
- [3] T. Belytschko, Y.Y. Lu, L. Gu, Element-free Galerkin methods, *Int. J. Numer. Methods Eng.* 37 (1994) 229–256.
- [4] J. Oliver, Modelling strong discontinuities in solid mechanics via strain softening constitutive equations, Part 2: numerical simulation, *Int. J. Numer. Methods Eng.* 39 (1996) 3601–3623.
- [5] T. Belytschko, T. Black, Elastic crack growth in finite elements with minimal remeshing, *Int. J. Numer. Methods Eng.* 45 (5) (1999) 601–620.
- [6] N. Moës, J. Dolbow, T. Belytschko, A finite element method for crack growth without remeshing, *Int. J. Numer. Methods Eng.* 46 (1999) 131–150.

- [7] J. Dolbow, An extended finite element method with discontinuous enrichment for applied mechanics, Ph.D. Thesis, Northwestern University, 1999.
- [8] J.M. Melenk, I. Babuška, The partition of unity finite element method: basic theory and applications, *Comput. Methods Appl. Mech. Eng.* 39 (1996) 289–314.
- [9] W.K. Liu, Y. Zhang, M. Ramirez, Multiple scale finite element methods, *Int. J. Numer. Methods Eng.* 32 (1991) 969–990.
- [10] T. Strouboulis, I. Babuška, K. Copps, The design and analysis of the generalized finite element method, *Comput. Methods Appl. Mech. Eng.* (2000), in press.
- [11] T. Belytschko, Y. Krongauz, D. Organ, M. Fleming, P. Krysl, Meshless methods: an overview and recent developments, *Comput. Methods Appl. Mech. Eng.* 139 (1996) 3–47.
- [12] M. Fleming, Y.A. Chu, B. Moran, T. Belytschko, Enriched element-free Galerkin methods for singular fields, *Int. J. Numer. Methods Eng.* 40 (1997) 1483–1504.
- [13] J.K. Knowles, N.M. Wang, On the bending of an elastic plate containing a crack, *J. Math. Phys.* 39 (4) (1960) 223–236.
- [14] G.C. Sih, *Mechanics of Fracture 3: Plates and Shells with Cracks*, Noordhoff International Publishing, The Netherlands, 1977.
- [15] I. Babuška, M. Rosenzweig, A finite element scheme for domains with corners, *Numer. Math.* 20 (1972) 1–21.
- [16] P. Grisvard, *Elliptic Problems in Nonsmooth Domains*, Pitman Publishing, Boston, 1985.
- [17] H. Sosa, J. Eischen, Computation of stress intensity factors for plate bending via a path-independent integral, *Eng. Fract. Mech.* 25 (4) (1986) 451–462.
- [18] B. Moran, C.F. Shih, Crack tip and associated domain integrals from momentum and energy balance, *Eng. Fract. Mech.* 127 (1987).
- [19] C.F. Shih, R.J. Asaro, Elastic-plastic analysis of cracks on bimaterial interfaces: part I—small scale yielding, *J. Appl. Mech.* 55 (1988) 299–316.
- [20] J. Dolbow, N. Moës, T. Belytschko, Modeling fracture in Mindlin–Reissner plates with the extended finite element method, 2000, in press.
- [21] K.J. Bathe, M.L. Bucelem, F. Brezzi, Displacement and Stress Convergence of Our MITC Plate Bending Elements, *Eng. Comput.* 7 (1990) 291–302.
- [22] H. Ewalds, R. Wanhill, *Fracture Mechanics*, Edward Arnold, New York, 1989.
- [23] Y. Sumi, C. Yang, Z. Wang, Morphological Aspects of Fatigue Crack Propagation, Part II—Effects of stress biaxiality and welding residual stresses, Technical Report, Yokohama National University, Japan, 1995.
- [24] M. Fleming, The element-free Galerkin method for fatigue and quasi-static fracture, Ph.D. Thesis, Northwestern University, 1997.
- [25] P.F. Joseph, F. Erdogan, Bending of a thin Reissner Plate with a Through Crack, *J. Appl. Mech.* 58 (1991) 842–846.
- [26] H. Boduroglu, F. Erdogan, Internal and Edge Cracks in a plate of finite width under bending, *J. Appl. Mech.* 50 (1983) 621–628.